# Structure of high-density amorphous water. I. X-ray diffraction study

A. Bizid
*Faculté des Sciences de Tunis, Campus Universitaire, 1060 Le Belvédère, Tunis, Tunisia*

L. Bosio and A. Defrain
*Laboratoire CNRS "Physique des Liquides et Electrochimie," ESPCI, 10 rue Vauquelin, 75231 Paris Cedex 05, France*

M. Oumezzine
*Faculté des Sciences et Techniques, 5000 Monastir, Tunisia*

(Received 21 January 1987; accepted 30 April 1987)

X-ray diffraction measurements up to momentum transfer $q = 16$ Å$^{-1}$ were performed at atmospheric pressure on both the high-density form of amorphous ice obtained by pressurization of crystalline ice $I_h$ at 77 K up to 2 GPa and the low-density form obtained by further heating. These two amorphous phases exhibit significant differences at the level of the second- and third-nearest neighbors which involve a decrease of the O–O–O angle on compression at high pressure. Moreover, it is found that the low-density form is quite similar to that obtained by vapor deposition on cooled substrates at 77 K.

## I. INTRODUCTION

Amorphous solids can be prepared using several methods, including direct condensation of vapor onto cold substrates or rapid cooling of the liquid below the glass-transition temperature which have been successfully used to obtain amorphous water.[1–3] Recently, Mishima *et al.* described a new method to prepare a high-density amorphous water either from ice $I_h$[4] or from low-density amorphous water.[5] As it has been pointed out,[6] the properties of amorphous ices are of particular interest, at least in two fields: first, in astrophysics since the noncrystalline forms of ice are presumably present in the solar system. Second, in biology, the formation of amorphous ices—and especially the low-density one—during the cryoprotection processes prevents the death and destruction of organic cells which are ineluctable during the normal freezing of water into ice $I_h$. To these observations one can add that, in spite of the intensive study concerning the pressure–temperature diagram of water, our knowledge of the structure or the mechanism between stable and metastable solid phases is still incomplete.

We here report the results of x-ray diffraction measurements of two amorphous varieties of water, studied at atmospheric pressure. They were obtained with heavy water so that the O–O correlations, which one can deduce, complete the neutron diffraction data (mainly induced by the D–D and O–D correlations) given in the next paper.[7]

## II. EXPERIMENTAL PROCEDURES

The high-density form of amorphous ice was obtained by pressurization of crystalline ice $I_h$, at 77 K, up to 2 GPa according to the procedure given by Mishima *et al.*[4] On removal of the pressure the metastable phase, which occured at high pressure, persisted down to zero pressure thus making the study feasible. Nevertheless a special device has to be designed to prepare the sample and to extract it before loading the sample holder, all these operations being performed at 77 K, i.e. in liquid nitrogen.

### A. Sample preparation

A piston–cylinder apparatus, made in maraging steel, could keep three positions in the tank filled with liquid nitrogen (Fig. 1). On position 1 the sample was squeezed between the plug and the piston to the desired pressure by applying a force provided by a hydraulic press. After release of the pressure, the piston–cylinder system was set on another seat (in position 2, Fig. 1) and the plug extracted by pushing the piston. Finally, in position 3, the sample could be ejected from the cylinder and fell in the sample holder.

During the pressure variation, the pressure was mea-

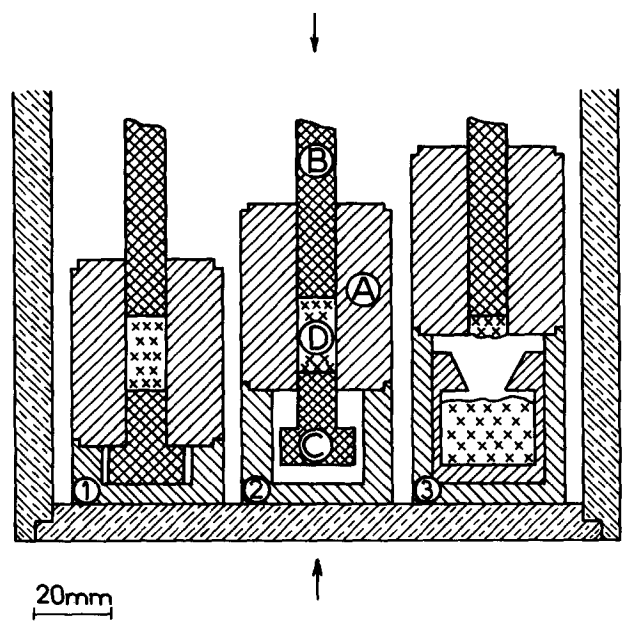


FIG. 1. Experimental device to obtain the high-density amorphous water. On seat 1 the sample is submitted to pressure. On seat 2 the plug can be extracted. In position 3 the sample is forced to fall inside the sample holder. All these operations are performed in liquid nitrogen (A: cylinder; B: piston; C: plug; D: sample).

 0021-9606/87/162225-06$02.10  

sured with both a Bourdon manometer and an electrical pressure transducer located in the primary oil circuit of the press. The piston displacement was determined by means of an electrical gauge so that the volume variation of the sample vs pressure could be plotted on an $X$–$Y$ recorder (the error due to friction was then assumed to be negligible).

For convenience sake, in our experiments and contrary to the previous experiments,[4,5] no indium cup was used to contain the sample: a volume of heavy water (NMR spectroscopy purity, isotopic enrichment: 99.8%), lower than 2 $cm^3$, was directly poured into the high pressure container. Figure 2 shows the piston displacement as a function of the nominal pressure for a $D_2O$ sample of 0.9655 g poured into a high pressure device of 10.0 mm i.d. On compression (Fig. 2, curve a) a volume decrease starts at about 1.1 GPa and appears complete by 1.7 GPa: this volume variation indicates the formation of the high-density form. By comparison to the values found for light water[4] it seems that deuteration has a negligible effect on such a transition. On pressure relaxation (Fig. 2, curve b), the transition is not reversible and a subsequent compression (curve c) does not show any effect (note that the hysteresis attached to a cycle of compression and decompression gives an indication on friction, thus estimated to be within 0.2 GPa at 1 GPa).

An establishment of the appearance of a new phase is given by differential thermal analysis performed on a small amount of the sample previously prepared (Fig. 3): on heating (rate $\sim 2$ K $min^{-1}$) a broad exothermic transition arises around 128 K; at higher temperatures, 162 and 167 K, respectively, two other exothermic transitions occur. X-ray measurements[8] indicate that the first transition corresponds to the formation of the low-density amorphous ice; at 162 K it transforms into $I_c$ ice which, in turn, reverts into the stable $I_h$ phase around 167 K. Finally, melting (endothermic peak) begins at 276 K.

### B. X-ray procedure

The x-ray data were collected by use of a standard diffractometer operating with a molybdenum tube ($\lambda = 0.7093$ Å) using the step-scanning method with steps equal to 0.1° ($2\theta$) in the 0.1–40° ($2\theta$) range and 0.25° ($2\theta$) at higher angles. Monochromatization was obtained with a bent asymmetric quartz monochromator placed in the incident beam. Scattered intensities were measured by a scintillation counter in conjunction with a pulse-height analyzer. Each angular range was studied and counts accumulated by repeated scanning until the statistical error was lower than 0.5% for all the noncrystalline phases examined.

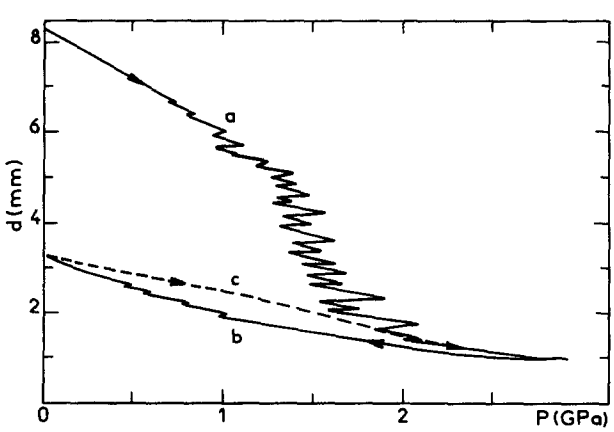


FIG. 2. The displacement of the piston inside the cylinder plotted against the applied pressure. The variation of the sample volume on the first compression (curve a) is the signature of the high-density ice formation. Subsequent compression (curve b) or recompression (curve c) shows no anomaly.

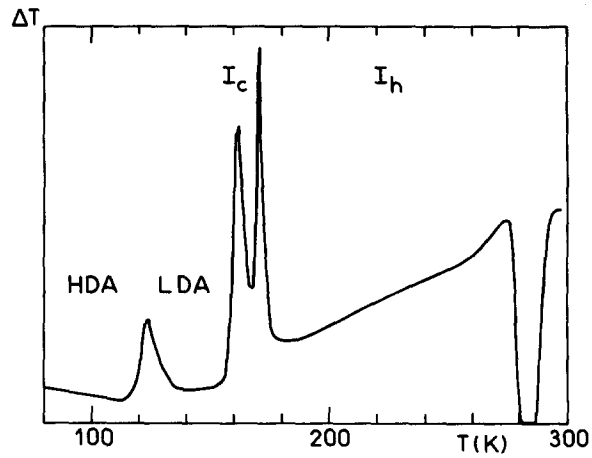


FIG. 3. Differential thermal analysis (HDA and LDA are the abbreviations for high- and low-density amorphous ices; $I_c$ and $I_h$ are the cubic and hexagonal crystalline forms).

Two kinds of sample holders were used: the first, specifically suited to momentum transfers $q = 4\pi \sin\theta/\lambda$ lower than 9 $Å^{-1}$, was an 8-mm-diam, 15-mm-high cylinder of aluminized Mylar (10 $\mu$m thick) wrapped inside a cylindrical copper block with two windows for the x-ray passage.[8] The second was a framework (5 mm thick, $20\times25$ $mm^2$ hollow): when operating in the moving sample transmission geometry it allowed x-ray diffraction measurements up to 16 $Å^{-1}$. In both cases, two plane beryllium windows, fastened to the copper block, allowed the passage of incident and diffracted x-ray beams and also maintained a uniform temperature of the inside samples. After attachment at 77 K, of one or the other sample holders within the previously cooled cryostat, the sample was maintained in vacuum.

Several samples were prepared but x-ray diffraction measurements often revealed spurious Bragg peaks at the $q$ values given in Table I; clearly, these peaks cannot be ascribed to a small amount of untransformed ice $I_h$. No correlation was found between the appearance of these Bragg reflections and the parameters capable of having an influence during the sample preparation (i.e., rate of pressure application, powder or single crystalline form of the initial $I_h$ sample, amount of compression–decompression cycles,...). We attribute the indesirable contamination of 95% of the samples to one or several high-pressure crystalline forms of ice since, after all, the transition under investigation takes place in a metastable regime. Moreover, when heating to 162 K, the spurious crystalline phases reverted to $I_c$ ice. In this study we succeeded in obtaining samples completely free from any crystalline material.

TABLE I. $q$ values of the powder reflections often observed in the high-density amorphous water (vw: very weak; w: weak; m: medium; s: strong; because of a probable preferred orientation of crystallities, the relative intensities exhibit some change from one sample to another). These reflections cannot be assigned to any high-pressure phase of ice presently known.

| $q = 2\pi/d_{hkl}$ (Å$^{-1}$) | Intensity |
|---|---|
| 1.61 | vw |
| 1.76 | vw |
| 2.12 | w |
| 2.28 | s |
| 2.38 | w |
| 2.79 | m |
| 3.39 | w |
| 3.83 | m |
| 4.06 | w |

### C. Data reduction

In order to obtain the effective scattering of the amorphous ices, a number of corrections must be applied to the intensities measured.[9]

(i) The background intensity and the Be Bragg peaks of the empty cell were measured with the same accuracy as that of amorphous materials.

(ii) Since the compactness of the samples was not well defined due to the method used to fill the cell at 77 K, the sample absorption was measured with the detector set at zero angle. Depending on the sample holder chosen (flat slab or cylinder) the adequate absorption factor was used to correct the sample absorption and to eliminate the Be windows scattering.

(iii) The polarization correction required by the use of a monochromator in the incident beam was applied.

(iv) Concerning the parasitic scattering, the incoherent scattering was calculated employing the theoretical Compton intensity,[10] $R^{-2}$ recoil factor, and the modified absorption factor.[9] The double scattering intensity was determined by the numerical integration method,[11] suited for a polarized incident beam (no correction was applied for the cylindrical sample [12]).

## III. STRUCTURE DETERMINATION

The determination of structural information for water using x-ray study is greatly facilitated by the fact that the distribution of electron density in a water molecule is almost spherical.[13] In such conditions the molecule can be treated as a homoatomic system, the pair correlation function thus yielding information about the molecular centers (actually not very different from oxygen atoms). In our data reduction we used the x-ray scattering amplitudes for water, written in an analytical form.[10]

The absolute intensity scale of the corrected intensity—thus the structure factor $S(q)$ of the material—was established using the Krogh-Moe and Norman method in conjunction with a refinement procedure which consisted in minimizing the oscillations of the pair-correlation function $g(r)$ for intermolecular distances lower than 2.0 Å, i.e., within a region where it is known that $g(r)$ is featureless.

### A. Low-density amorphous water

Inverting the chronological order of the measurements, let us begin with the description of the structure of the low-density ice—that is, the structure of the phase formed after heating the decompressed sample slightly beyond the first exothermic peak shown in Fig. 3 and subsequently cooled to 77 K—in order to compare its molecular arrangement to that known and previously studied[1] using a sample obtained by vapor deposition on cooled substrates.

The structure factor as determined in our experiments is shown in Fig. 4 (solid line) together with the curve deduced from the tabulated intensity[1] and related to a sample deposited and studied at 77 K (dotted line). Despite the fact that heavy and light water were used, the analogy of the two curves is evident: even the hump on the right side of the third maximum is reproduced. Clearly, the two methods of sample preparation lead to the same amorphous phase. The values of $S(q)$ in the $q$ range 0.2–16 Å$^{-1}$ are listed in Table II.

The Fourier inversion of the structure factor gives the pair distribution function $g(r)$ of the molecular centers;

$$g(r) = 1 + \frac{1}{2\pi^2\rho}\int q^2[S(q) - 1]\sin qr\, dq,$$

where the density $\rho$ is, in this case, kept equal to 0.031 mol. Å$^{-3}$.

Since the scattering function still oscillates near the upper limit ($q_m = 16$ Å$^{-1}$) the termination effect of the experimental intensity was avoided using the Hanning modification function $\frac{1}{2}[1 + \cos(\pi q/q_m)]$. Figure 5 displays the weighted function $4\pi r\rho[g(r) - 1]$ of the low-density amorphous ice. It appears that the first nearest neighbors, located at the mean value of 2.8 Å, are clearly separated from the second ones; the coordination number, inferred from the ra-

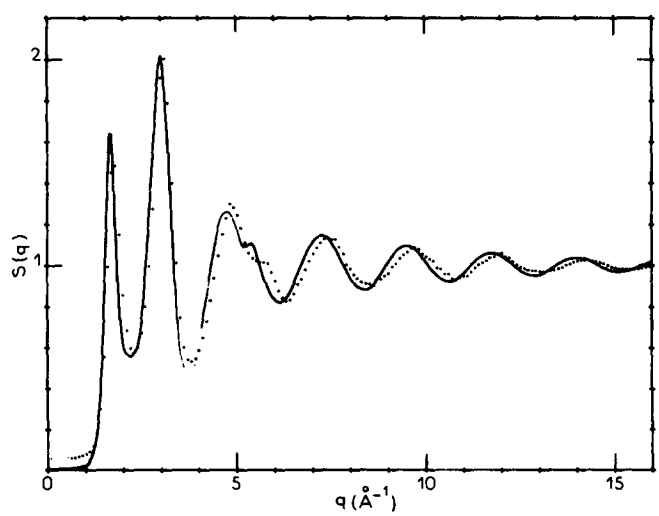


FIG. 4. The structure factor for low-density amorphous water. Solid line: present work ($D_2O$). Dotted line: amorphous water ($H_2O$) obtained by vapor deposition on substrate cooled at 77 K (Ref. 1); the shift towards the high momentum transfers of the dotted curve is due to a smaller oxygen–oxygen distance found equal to 2.76 Å against 2.80 Å in our measurements.

TABLE II. Molecular center structure factor $S(q)$ of low- and high-density amorphous water.

| $q$ | $S_{LD}$ | $S_{HD}(q)$ | $q$ | $S_{LD}(q)$ | $S_{HD}(q)$ | $q$ | $S_{LD}(q)$ | $S_{HD}(q)$ |
|---|---|---|---|---|---|---|---|---|
| 0.20 | 0.005 | 0.006 | 4.10 | 0.705 | 0.846 | 10.10 | 0.998 | 0.998 |
| 0.30 | 0.005 | 0.006 | 4.20 | 0.816 | 0.903 | 10.20 | 0.972 | 0.973 |
| 0.40 | 0.006 | 0.006 | 4.30 | 0.935 | 0.947 | 10.30 | 0.950 | 0.952 |
| 0.50 | 0.006 | 0.007 | 4.40 | 1.055 | 0.987 | 10.40 | 0.940 | 0.934 |
| 0.60 | 0.007 | 0.007 | 4.50 | 1.161 | 1.020 | 10.50 | 0.931 | 0.926 |
| 0.70 | 0.009 | 0.009 | 4.60 | 1.224 | 1.056 | 10.60 | 0.925 | 0.919 |
| 0.80 | 0.012 | 0.011 | 4.70 | 1.253 | 1.089 | 10.70 | 0.924 | 0.926 |
| 0.90 | 0.016 | 0.014 | 4.80 | 1.264 | 1.110 | 10.80 | 0.933 | 0.935 |
| 1.00 | 0.022 | 0.017 | 4.90 | 1.237 | 1.136 | 10.90 | 0.945 | 0.947 |
| 1.10 | 0.040 | 0.021 | 5.00 | 1.189 | 1.153 | 11.00 | 0.961 | 0.962 |
| 1.20 | 0.088 | 0.027 | 5.10 | 1.125 | 1.164 | 11.10 | 0.977 | 0.976 |
| 1.30 | 0.159 | 0.036 | 5.20 | 1.087 | 1.186 | 11.20 | 1.003 | 1.001 |
| 1.40 | 0.355 | 0.052 | 5.30 | 1.097 | 1.190 | 11.30 | 1.021 | 1.021 |
| 1.50 | 0.749 | 0.075 | 5.40 | 1.105 | 1.174 | 11.40 | 1.031 | 1.038 |
| 1.55 | 1.076 | 0.080 | 5.50 | 1.085 | 1.134 | 11.50 | 1.048 | 1.048 |
| 1.60 | 1.421 | 0.115 | 5.60 | 1.023 | 1.032 | 11.60 | 1.057 | 1.060 |
| 1.65 | 1.639 | 0.193 | 5.70 | 0.960 | 0.945 | 11.70 | 1.067 | 1.061 |
| 1.70 | 1.638 | 0.301 | 5.80 | 0.907 | 0.884 | 11.80 | 1.058 | 1.060 |
| 1.75 | 1.459 | 0.433 | 5.90 | 0.867 | 0.847 | 11.90 | 1.060 | 1.059 |
| 1.80 | 1.223 | 0.597 | 6.00 | 0.840 | 0.821 | 12.00 | 1.046 | 1.044 |
| 1.85 | 1.014 | 0.782 | 6.10 | 0.820 | 0.801 | 12.10 | 1.038 | 1.039 |
| 1.90 | 0.848 | 0.951 | 6.20 | 0.822 | 0.816 | 12.20 | 1.025 | 1.025 |
| 1.95 | 0.718 | 1.096 | 6.30 | 0.839 | 0.833 | 12.30 | 1.010 | 1.009 |
| 2.00 | 0.630 | 1.252 | 6.40 | 0.861 | 0.862 | 12.40 | 0.989 | 0.991 |
| 2.05 | 0.588 | 1.442 | 6.50 | 0.895 | 0.897 | 12.50 | 0.973 | 0.971 |
| 2.10 | 0.572 | 1.615 | 6.60 | 0.943 | 0.946 | 12.60 | 0.968 | 0.968 |
| 2.15 | 0.562 | 1.687 | 6.70 | 0.984 | 0.985 | 12.70 | 0.953 | 0.952 |
| 2.20 | 0.557 | 1.640 | 6.80 | 1.034 | 1.035 | 12.80 | 0.953 | 0.950 |
| 2.25 | 0.561 | 1.531 | 6.90 | 1.079 | 1.075 | 12.90 | 0.946 | 0.951 |
| 2.30 | 0.571 | 1.418 | 7.00 | 1.107 | 1.108 | 13.00 | 0.951 | 0.952 |
| 2.35 | 0.582 | 1.302 | 7.10 | 1.136 | 1.136 | 13.10 | 0.957 | 0.959 |
| 2.40 | 0.604 | 1.170 | 7.20 | 1.142 | 1.143 | 13.20 | 0.970 | 0.966 |
| 2.45 | 0.649 | 1.043 | 7.30 | 1.149 | 1.149 | 13.30 | 0.980 | 0.982 |
| 2.50 | 0.721 | 0.956 | 7.40 | 1.136 | 1.131 | 13.40 | 0.989 | 0.992 |
| 2.55 | 0.817 | 0.917 | 7.50 | 1.118 | 1.111 | 13.50 | 1.005 | 1.005 |
| 2.60 | 0.938 | 0.910 | 7.60 | 1.082 | 1.081 | 13.60 | 1.020 | 1.018 |
| 2.65 | 1.086 | 0.928 | 7.70 | 1.051 | 1.056 | 13.70 | 1.032 | 1.023 |
| 2.70 | 1.241 | 0.978 | 7.80 | 1.010 | 1.017 | 13.80 | 1.038 | 1.031 |
| 2.75 | 1.386 | 1.054 | 7.90 | 0.985 | 0.879 | 13.90 | 1.036 | 1.036 |
| 2.80 | 1.525 | 1.136 | 8.00 | 0.946 | 0.946 | 14.00 | 1.041 | 1.040 |
| 2.85 | 1.678 | 1.219 | 8.10 | 0.912 | 0.915 | 14.10 | 1.039 | 1.033 |
| 2.90 | 1.840 | 1.304 | 8.20 | 0.894 | 0.897 | 14.20 | 1.031 | 1.037 |
| 2.95 | 1.969 | 1.388 | 8.30 | 0.881 | 0.883 | 14.30 | 1.029 | 1.026 |
| 3.00 | 2.018 | 1.457 | 8.40 | 0.877 | 0.877 | 14.40 | 1.019 | 1.021 |
| 3.05 | 1.978 | 1.493 | 8.50 | 0.889 | 0.888 | 14.50 | 1.004 | 1.005 |
| 3.10 | 1.872 | 1.489 | 8.60 | 0.896 | 0.900 | 14.60 | 0.994 | 0.993 |
| 3.15 | 1.731 | 1.444 | 8.70 | 0.924 | 0.924 | 14.70 | 0.989 | 0.990 |
| 3.20 | 1.569 | 1.357 | 8.80 | 0.947 | 0.945 | 14.80 | 0.979 | 0.975 |
| 3.25 | 1.396 | 1.245 | 8.90 | 0.976 | 0.974 | 14.90 | 0.969 | 0.969 |
| 3.30 | 1.220 | 1.128 | 9.00 | 1.010 | 1.011 | 15.00 | 0.970 | 0.970 |
| 3.35 | 1.047 | 1.010 | 9.10 | 1.038 | 1.034 | 15.10 | 0.969 | 0.973 |
| 3.40 | 0.884 | 0.889 | 9.20 | 1.064 | 1.063 | 15.20 | 0.971 | 0.967 |
| 3.45 | 0.739 | 0.773 | 9.30 | 1.086 | 1.081 | 15.30 | 0.973 | 0.976 |
| 3.50 | 0.626 | 0.692 | 9.40 | 1.096 | 1.088 | 15.40 | 0.975 | 0.978 |
| 3.55 | 0.555 | 0.660 | 9.50 | 1.093 | 1.101 | 15.50 | 0.989 | 0.983 |
| 3.60 | 0.516 | 0.660 | 9.60 | 1.089 | 1.090 | 15.60 | 0.989 | 0.988 |
| 3.70 | 0.481 | 0.671 | 9.70 | 1.085 | 1.082 | 15.70 | 1.000 | 1.004 |
| 3.80 | 0.478 | 0.709 | 9.80 | 1.066 | 1.064 | 15.80 | 1.004 | 1.004 |
| 3.90 | 0.515 | 0.754 | 9.90 | 1.051 | 1.043 | 15.90 | 1.018 | 1.013 |
| 4.00 | 0.587 | 0.801 | 10.00 | 1.026 | 1.018 | 16.00 | 1.017 | 1.016 |

dial distribution function $4\pi r^2 \rho g(r)$, is equal to 4.0. No peak is observed near 3.3 Å, a level where the amorphous ice, prepared by a slow deposition of vapor onto a substrate cooled at 10 K, exhibits a small but well-resolved maximum.[1]

The second nearest-neighbors distance, around 4.6 Å, indicates a local tetrahedral configuration of the oxygen atoms.

### B. High-density amorphous water

Figure 6 displays the structure factor of the high-density form of amorphous water (i.e., the phase obtained immedi-

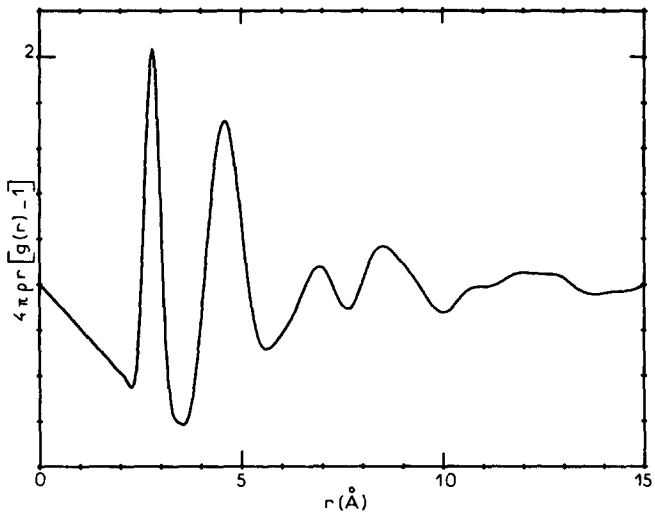


FIG. 5 The weighted pair correlation function of low-density amorphous ice against $r$.

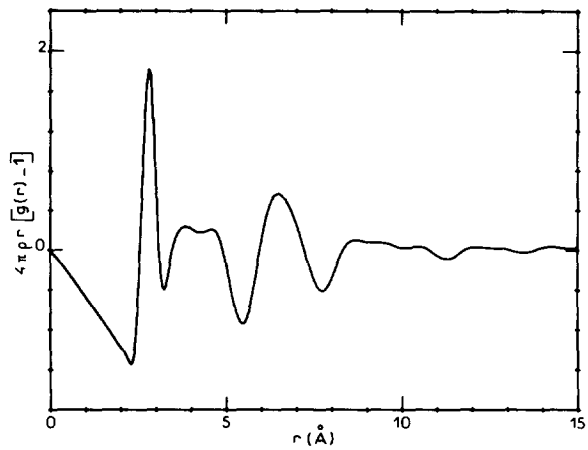


FIG. 7. The weighted pair-correlation function of high-density amorphous water vs $r$.

ately after compression of $I_h$ ice and decompression to zero pressure, at 77 K). Compared to the data given above, $S(q)$ exhibits significant differences both in the shapes and positions of the first maxima in the low-$q$ range. On the contrary, the structure factors of both forms of amorphous ice are quite similar in the high-$q$ range ($q > 7$ Å$^{-1}$). The values of $S(q)$ are listed in Table II.

Figure 7 shows the weighted function $4\pi r\rho[g(r) - 1]$ vs $r$, using once more the Hanning modification function. The first neighbors are found at approximately the mean distance 2.8 Å, that is, at the same distance as in the previously studied form of ice. However, the first shell is less well resolved. The second shell is broad and split into two peaks located near 3.7 and 4.65 Å.

In order to make more evident the structural differences between the two modifications of amorphous ice we have computed the differential function

$$4\pi r\{\rho_{HD}[g_{HD}(r) - 1] - \rho_{LD}[g_{LD}(r) - 1]\},$$

(the subscripts HD and LD refer to the high and low density forms). This function, drawn in Fig. 8, was calculated directly by Fourier transformation of $\Delta S(q) = S_{HD}(q) - S_{LD}(q)$; since $\Delta S(q)$ goes to zero beyond $q > 7$ Å$^{-1}$ (see inset in Fig. 8), as a consequence of the similarity of the structure factors in high-$q$ range, no truncation effect has to be introduced during the Fourier transformation. The first conclusion which can be drawn from Fig. 8 is a confirmation that the first coordination shells are identical in the two amorphous forms of ice (the negative slope of the curve in the 0–3 Å range is due to the density differences). The second conclusion is that the main difference appears at the level of the second and subsequent nearest neighbors; the maximum in the differential function around 3.6 Å can be attributed to a tendency of the second neighbors in high-density amorphous water to move close.

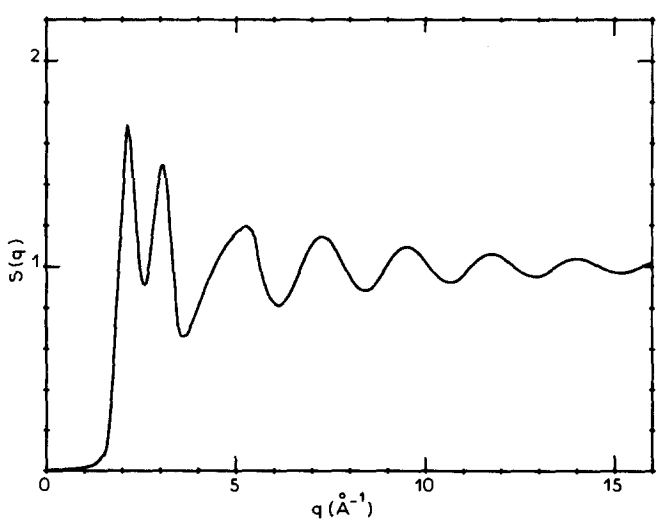


FIG. 6. The structure factor of high-density amorphous water obtained by compressing hexagonal ice to 2 GPa at 77 K.

## IV. CONCLUDING REMARKS

For the present, we shall not go into detail on the structure of the two kinds of amorphous water, postponing the discussion for the next paper[7] concerning the neutron scattering experiments, which provides complementary information on the O–D and D–D correlations. Nevertheless, we can immediately assert that the high-density form prepared at high pressure is different from that prepared by vapor deposition onto substrates cooled at 10 K. In the deposited sample, the increased density cannot be ascribed to a new structure but rather to a consequence of the deposition process which leads to a nontetrahedral[14] or interstitial[1] packing with extra molecules frozen in voids. On the contrary, in the high-pressure amorphous ice, the distribution of O–O atoms at the level of the second shell involves severe distortions and a decrease of the O–O–O angle with probably some break of hydrogen bonds. A model assuming the existence of finite H-bonded clusters (maybe with nontetrahedral angles) and a lot of non-H-bonded close pairs of molecules is suggested by Hadju[15]. In this sense, it would be imperative to examine if the transition between the low- and high-den-

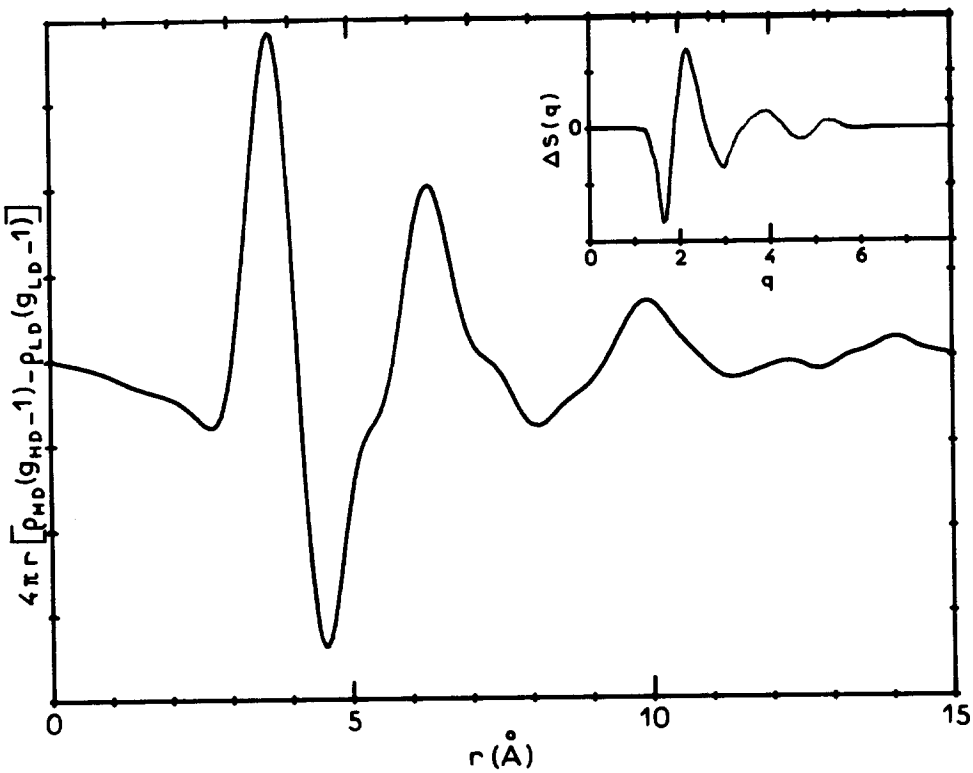


FIG. 8. A plot vs $r$ of the differential function $4\pi r\{\rho_{HD}[g_{HD}(r)-1]-\rho_{LD}[g_{LD}(r)-1]\}$ between the two forms of amorphous solids.

sity amorphous ices is a really reversible transition or if interconversion of the two metastable amorphous solids requires dissimilar and irreversible thermodynamics paths.[16] Clearly the key element is the hydrogen bonds behavior during the transition but at our present level of understanding we cannot answer the question whether the pressure-induced amorphization occurs by melting and refreezing along the extrapolated $I_h$ melting curve [4] rather than by a collapse of crystalline long-range order and of hydrogen-bonded structure[16].

## ACKNOWLEDGMENTS

We would particularly wish to thank G. P. Johari and J. Teixeira, who were at the origin of this study. We would also like to thank E. Whalley for helpful discussion and valuable comments.

[1] A. H. Narten, C. G. Venkatesh, and S.A. Rice, J. Chem. Phys. **64**, 1106 (1976).
[2] E. Mayer and P. Bruggeler, Nature (London) **298**, 715 (1982).
[3] J. Dubochet and J. Lepault, J. Phys. Paris **C7**, 85 (1984).
[4] O. Mishima, L. D. Calvert, and E. Whalley, Nature (London) **310**, 393 (1984).
[5] O. Mishima, L. D. Calvert, and E. Whalley, Nature (London) **314**, 76 (1985).
[6] J. P. Poirier, Nature (London) **314**, 12 (1985).
[7] M. C. Bellissent-Funel, L. Bosio, and J. Teixeira, J. Chem. Phys. **87**, 2231 (1987).
[8] L. Bosio, G. P. Johari, and J. Teixeira, Phys. Rev. Lett. **56**, 460 (1986).
[9] F. Hajdu and G. Palinkas, J. Appl. Crystallogr. **5**, 395 (1972).
[10] F. Hajdu, Acta Crystallogr. Sect. A **28**, 250 (1972).
[11] G. Mallet, C. Cabos, A. Escandre, and P. Delord, J. Appl. Crystallogr. **6**, 139 (1973).
[12] G. D. Wignall, J. A. J. Jarvis, W. E. Munsill, and C. J. Pings, J. Appl. Crystallogr. **7**, 366 (1974).
[13] A. H. Narten and H. A. Levy, J. Chem. Phys. **55**, 2263 (1971).
[14] F. Hajdu, Acta Chim. Budapest **96**, 355 (1978).
[15] F. Hajdu (private communication).
[16] G. P. Johari and S. J. Stones, Philos. Mag. **54**, 311 (1986).